ADVANCED ENERGY MATERIALS
www.advenergymat.de

Compositional Gradient of Mixed Halide 2D Perovskite Interface Boosts Outdoor Stability of Highly Efficient Perovskite Solar Cells

*Matteo Degani, Riccardo Pallotta, Giovanni Pica, Masoud Karimipour, Alessandro Mirabelli, Kyle Frohna, Miguel Anaya, Tianyu Xu, Chang-Qi Ma, Samuel D. Stranks, Monica Lira Cantù, and Giulia Grancini**

Interface engineering using self-assembled 2D perovskite interfaces is a consolidated route to efficient and durable perovskite solar cells. Whether the 2D perovskite forms a homogeneous conformal layer or is heterogeneously distributed on the surface, interface defects are passivated, leading to a general improvement in the device's open circuit voltage (V_{OC}) and stability. Here, an innovative strategy is developed for manipulating the composition of the 2D/3D perovskite interface that results in the formation of a gradient halide distribution, which extends from the surface to the bulk. The use of a bromide-based 2D perovskite triggers a progressive Br/I exchange, affecting not only the surface but also the perovskite underneath. As a result, not only the device V_{OC} improve, as expected, but also the photogenerated current is boosted, leading to a device efficiency of up to 24.4%. Such mixed halide gradient effectively passivates surface and bulk defects making the perovskite active layer more efficient and robust, as demonstrated by the superior device stability showing zero losses in performances upon 36 days (more than 800 h) test in outdoor conditions, those ones relevant for a marketable product.

1. Introduction

Surface passivation of 3D perovskite with an interfacial 2D perovskite layer is a common and effective strategy to improve device longevity while simultaneously boosting device power conversion efficiency (PCE). Owing to their layered structure, superior hydrophobicity and thermostability have been demonstrated.[1,2] Concomitantly, 2D perovskite passivates surface defects,[3] reducing non-radiative recombination losses, and thus improving both open circuit voltage (V_{OC}) and Fill Factor (FF).[4] This passivation effect occurs regardless of whether the 2D perovskite forms a continuous or a non-uniform distributed one, or even if it does not form at all, leaving the organic salts acting as surface modifiers. Different organic moieties have been tested for 2D passivation,[5] consisting of aromatic, aliphatic, or even ad hoc functionalized molecules. To form the salt precursor, the organic unit is bound to a halogen atom, which is most commonly iodine.[5]

By contrast, here we screen different halogens (I, Br, Cl) forming a 4-methylphenethylammonium X salt (MPEAX, X = Br, I, Cl), which we dispersed on top of a formamidinium based ($FAPbI_3$) perovskite surface. Solar cells treated with MPEAX salts showed

M. Degani, R. Pallotta, G. Pica, G. Grancini
Department of Chemistry & INSTM
Università di Pavia
Via T. Taramelli 14, Pavia 27100, Italy
E-mail: giulia.grancini@unipv.it

M. Karimipour, M. L. Cantù
Catalan Institute of Nanoscience and Nanotechnology (ICN2)
CSIC and the Barcelona Institute of Science and Technology (BIST)
Building ICN2
Campus UAB
Bellaterra, Barcelona 08193, Spain

The ORCID identification number(s) for the author(s) of this article can be found under https://doi.org/10.1002/aenm.202404469

© 2024 The Author(s). Advanced Energy Materials published by Wiley-VCH GmbH. This is an open access article under the terms of the Creative Commons Attribution License, which permits use, distribution and reproduction in any medium, provided the original work is properly cited.

DOI: 10.1002/aenm.202404469

A. Mirabelli, K. Frohna, M. Anaya, S. D. Stranks
Department of Chemical Engineering and Biotechnology
University of Cambridge
Philippa Fawcett Drive, Cambridge CB3 0AS, UK

M. Anaya
Departamento de Fisica de la Materia Condensada
Insituto de ciencia de Materiales de Sevilla
Universidad de Sevilla-CSIC
Avenida Reina Mercedes SN, Sevilla 41012, Spain

T. Xu, C.-Q. Ma
Innovation Laboratory & Printable Electronics Research CenterSuzhou
Institute of Nano-Tech and Nano-Bionics (SINANO)Chinese Academy of Sciences (CAS)Ruoshui Road 398
Suzhou 215123, China

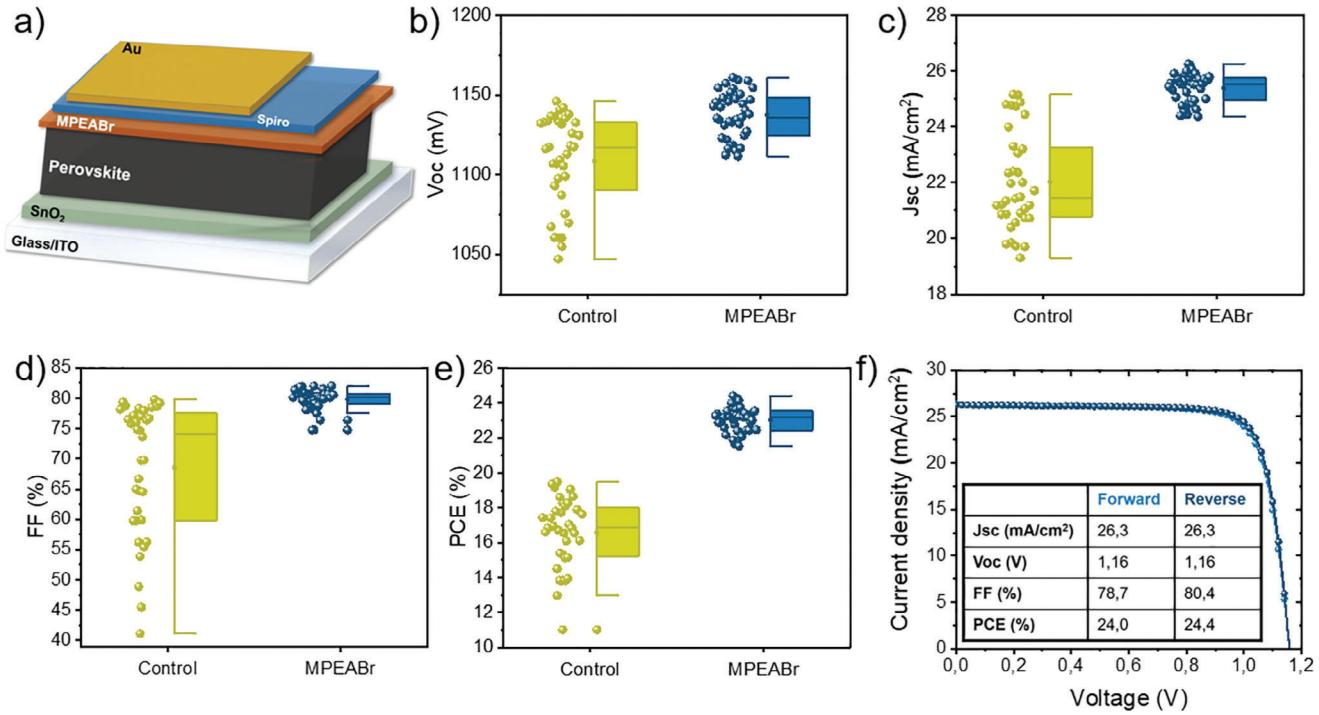

Figure 1. Photovoltaic performance of the passivated PSC. a) Schematic illustration of a stack of the passivated PSC. PV parameters b) Voc, c) Jsc, d) FF and e) PCE. Characteristic JV curve of the best-passivated device.

increased V_{OC} compared with the non treated ones, due to surface trap passivation. Interestingly, when Br-based salt is used, Br/I exchange is induced,[6] leading to a compositional halide gradient, which extends from the surface to the perovskite bulk. The 2D perovskite consists of a mixture of $MPEAPb_2(I_xBr_{1-x})_4$ with a Br gradient concentration that starts low at the surface and increases deeper in the perovskite bulk. As a result, surface but also bulk passivation occurs, enhancing device V_{OC} and FF at one side, and device photocurrent at the other, ultimately leading to a champion PCE device of 24.4%. Our innovative strategy demonstrates that due to the soft nature of the perovskite structure, a surface passivation method can also perturb the active layer bulk. The resulting compositional gradient extends through one third of the bulk thickness of the perovskite layer, with a concomitant boost of the surface and bulk material properties. Device longevity is remarkably enhanced, as tested under outdoor conditions for 850 h, which means more than 800 h, which are those ones relevant for a marketable product, making up a reliable proof of concept potentially relevant to shorten the time to market for perovskite photovoltaics.

2. Results and Discussion

Figure 1a shows a schematic representation of the fabricated solar cell architecture in *nip* configuration. $FAPbI_3$ is sandwiched in between tin oxide (SnO_2) as the electron transport layer (ETL) and spiro-OMeTAD as the hole transporting layer (HTL). Here we use a commercial colloidal solution of SnO_2 employing bulk passivation agents in the SnO_2 matrix as a consolidated way to improve the material quality (see details in Figure S1, Supporting Information) and, therefore, the device interface.[7] To engineer the perovskite/HTL interface, we employ a 4-methylphenethylammonium X salt (MPEAX, X = Br, I, Cl) dissolved in isopropyl alcohol (IPA) as the precursor for the in situ formation of a 2D perovskite layer. Upon screening different halides, we focus our optimization on Br- based salt used as a passivation layer, given the highest performances reached (see Figures S2 and S3, Supporting Information). Figure 1b–e shows the photovoltaic (PV) parameters of the resulting device upon MPEABr surface passivation. First, we observe a narrower distribution of all photovoltaic (PV) parameters with respect to the control devices, indicative of a highly reproducible passivation method, with a concomitant improvement in the device V_{OC}, short circuit current (J_{SC}) and FF across the 35 investigated devices. PCE above 24% has been reached (Figure 1f), with no hysteresis in the current-voltage characteristics and without loss in the stabilized power output (Figure S4a, Supporting Information). As expected, surface passivation actively improves device FF and V_{OC}, as is commonly observed in this type of junction.[4] Notably, device FF as high as 82% have been reached, demonstrating that our high-quality device interfaces minimize resistive loss channels.[8] By contrast, the observed improvement in the device (short circuit current density) J_{SC} (confirmed by Incident Photon to Current Efficiency, IPCE, Figure S4b, Supporting Information) of more than 15% is unexpected. To give a rational explanation of this behavior, we have first investigated the 2D processing conditions, focusing on – the effect of the surface thermal treatment in the 2D formation.[9–11] For the device shown in Figure 1 there is no post-treatment annealing step, resulting in a slower interaction between the organic salt and the perovskite surface. Figure S5 (Supporting Information), by contrast, reports the photovoltaic (PV)903083 parameters of the same device

© 2024 The Author(s). Advanced Energy Materials published by Wiley-VCH GmbH

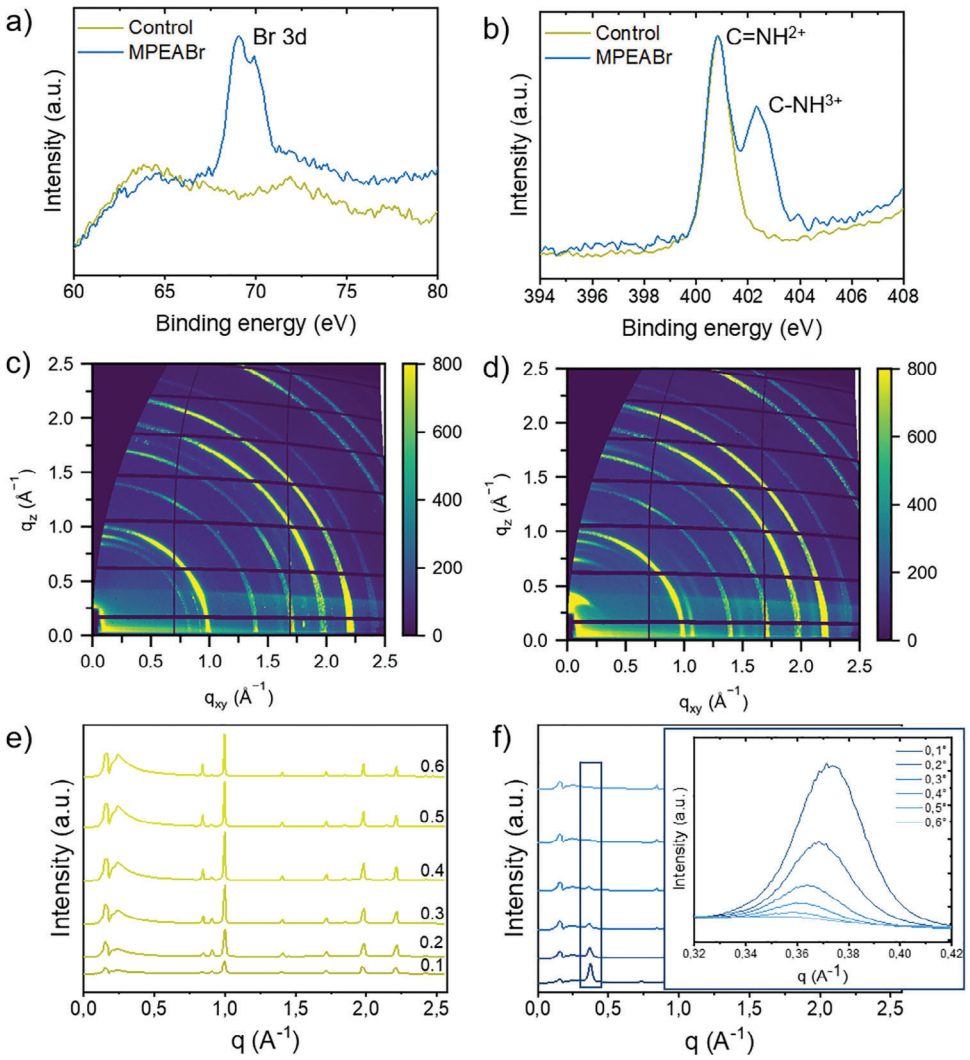

Figure 2. Structural analysis of perovskite thin films. Core level XPS spectra of the a) Br 3d b) N 1s. 2D GIWAXS patterns respectively of the c) control and of the d) passivated sample. Intensity versus q in the out-of-plane direction with different incident angles of the e) control and f) MPEABr sample with a magnification where the peak of 2D perovskite is present.

including an annealing step after the surface treatment. The annealing step slightly improves the V_{OC}, while the J_{SC} dramatically reduces as well as the device FF, leading to an overall reduction in the performances. The formation of a more compact 2D layer induced by annealing is in this case detrimental, possibly related to the formation of an extraction barrier at the interface, limiting the J_{SC} and the FF, in agreement with other recent literature reports.[12]

To elucidate the reason behind the net gain in the device performances for the passivated devices without any annealing step, specifically for FF and J_{SC}, we employed a combination of surface-sensitive techniques with optoelectronic device characterization. First, to understand the reasons behind the FF improvement, we performed a transient photocurrent (TPC) analysis, as shown in Figure S6a (Supporting Information). The TPC data show a longer decay time for the control (of 5.08 µs) compared to the MPEABr -2D treated sample (of 2.11 µs), indicating a faster charge extraction for the latter, which can explain the FF improvement.[13] The slower decay in the transient photovoltage (TPV) for the MPEABr -2D treated device, as shown in Figure S6b (Supporting Information), with respect to the control, indicates a lower recombination rate, which can explain the V_{OC} enhancement. A shorter carrier lifetime is indeed the result of higher non-radiative charge recombination, in agreement with the PV parameters.[14]

To understand the reason behind the different PV parameters, we elucidate the structural/chemical properties of the MPEABr treated sample. First, we analyzed the surface composition of the MPEABr treated film by means of X-ray photoelectron spectroscopy (XPS). Results are shown in **Figure 2**a,b (Figure S7 for the MPEABr annealed device, Supporting Information) where we identified the Br 3d[15] peak at 69 eV, and the C—C—NH^{3+} peak at 402.3 eV, ascribed to the organic salt,[16] confirming the presence of the MPEABr on the surface. The peak at 400.8 eV is related to C═NH^{2+}[17] moiety on the FA cation. Additionally, ultraviolet photoelectron spectroscopy (UPS) has been applied to retrieve

© 2024 The Author(s). Advanced Energy Materials published by Wiley-VCH GmbH

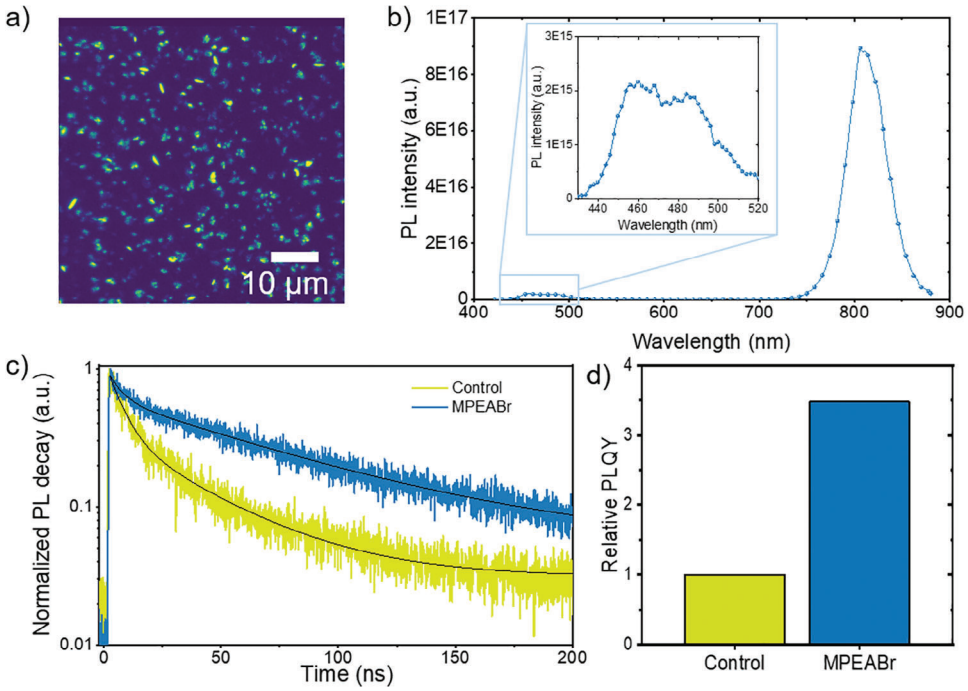

Figure 3. Optical measurement on perovskite thin films. a) 60 × 60 μm PL map of the MPEABr passivated perovskite excited at 405 nm and collected at 450 nm. b) PL spectrum of the low dimensional perovskite and inset a zoom in the 435–520 nm region showing the emission from the 2D perovskite. c) Time decays of the PL signal for both reference and 4-MPEABr thin film on glass d) PLQY of both reference and MPEABr samples.

the energy band diagram of the perovskite (Figure S8, Supporting Information).[18] The surface energetics shifted from −4.18 CB and −5.69 VB for the control sample to −3.87 CB and −5.38 VB for the MPEABr sample, indicating a structural modification induced by the Br passivation. As a result, the energy band alignment allowed for a better charge extraction, which reflected the higher J_{SC} and FF.

To better understand the structural composition, we performed grazing incidence wide-angle X-ray scattering (GIWAXS) measurements on both the control and passivated films (Figure 2c,d,e,f, respectively). The passivated sample shows a peak ≈q = 0.37 $Å^{-1}$ (absent in the control), which is related to the formation of a 2D perovskite layer. Additionally, from the diffractogram, we observe a preferential horizontal stacking orientation of the spacer cation in the passivated sample, as the diffraction peak is stronger in the out-of-plane direction. To gather information on the 2D perovskite distribution as a function of depth, we measured the GIWAXS pattern at increasing X-ray incident angles, allowing us to analyze deeper within the bulk of the halide perovskite. Going deeper, we observe a progressive decrease in the intensity of the peak associated with the 2D. The 2D peak is detectable up to an incident X-ray angle of 0.4° (Figure 2f). By working out of the X-ray penetration depth, we estimate that the above-mentioned peak is discernible up to 170 nm into the bulk of the sample.[19] The penetration of Br into the $FAPbI_3$ layer was confirmed by Time-of-Flight Secondary Ion Mass Spectrometry (ToF-SIMS, Figure S9, Supporting Information). This indicates that while the 2D perovskite is mainly located at the surface, it has also penetrated deeper in the bulk of the perovskite absorber. To better understand the chemical nature of the 2D layer, we monitored the 2D peak position as a function of incident angle. As the X-rays probe deeper in the sample the peak shifts from 0.375 to 0.36 $Å^{-1}$ (Figure 2f). This result suggests a compositional difference between the perovskite surface and the bulk underneath. In particular, the shift is consistent with a gradual change going from a $MPEAPb_2(I_xBr_{1-x})_4$ at the surface, to 2D with a higher Br content deeper in the bulk. Notably, this shift is consistent with XRD results of pure $MPEA_2PbI_4$ and $MPEA_2PbBr_4$ (Figure S10, Supporting Information).[20]

To further verify the surface passivation effect and the presence of the $MPEAPb_2(I_xBr_{1-x})_4$, we measured the hyperspectral Photoluminescence (PL) signal by mapping the nanodistribution of the PL signal from the 2D phase, as well as the bulk PL lifetime and Quantum Yield (PLQY).

From the PL map, specifically collected at 450 nm to monitor the emission from the wide band gap 2D $MPEAPb_2(I_xBr_{1-x})_4$, we observe a spatially non-uniform signal over the whole surface of the treated sample (**Figure 3**a), instead absent in the reference thin film (Figure S12, Supporting Information). Notably, despite the observation that the nanoscale distribution of the 2D perovskite emission is not uniform across the surface, its effect is beneficial,[3] contributing to the ongoing debate on whether a conformal layer of 2D perovskite is better over a non-conformal one.[21] The full PL spectra at those regions (Figure 3b) display a major peak above 800 nm, which is assigned to the $FAPbI_3$ emission. At shorter wavelengths, we observe a double peak at 460 and 490 nm, as shown in the magnification in Figure 3b. This broad peak can be attributed to the emission from $MPEA_2Pb(I_{1-x}Br_x)_4$ mixed-halide phases. Interestingly, this observation indicates that the Br can infiltrate in the octahedra creating a mixed 2D phase, in agreement with the GIWAXS data. Indeed, the PL shifts from both the pure iodide 2D emission at 520 nm,[22] and the pure

© 2024 The Author(s). Advanced Energy Materials published by Wiley-VCH GmbH

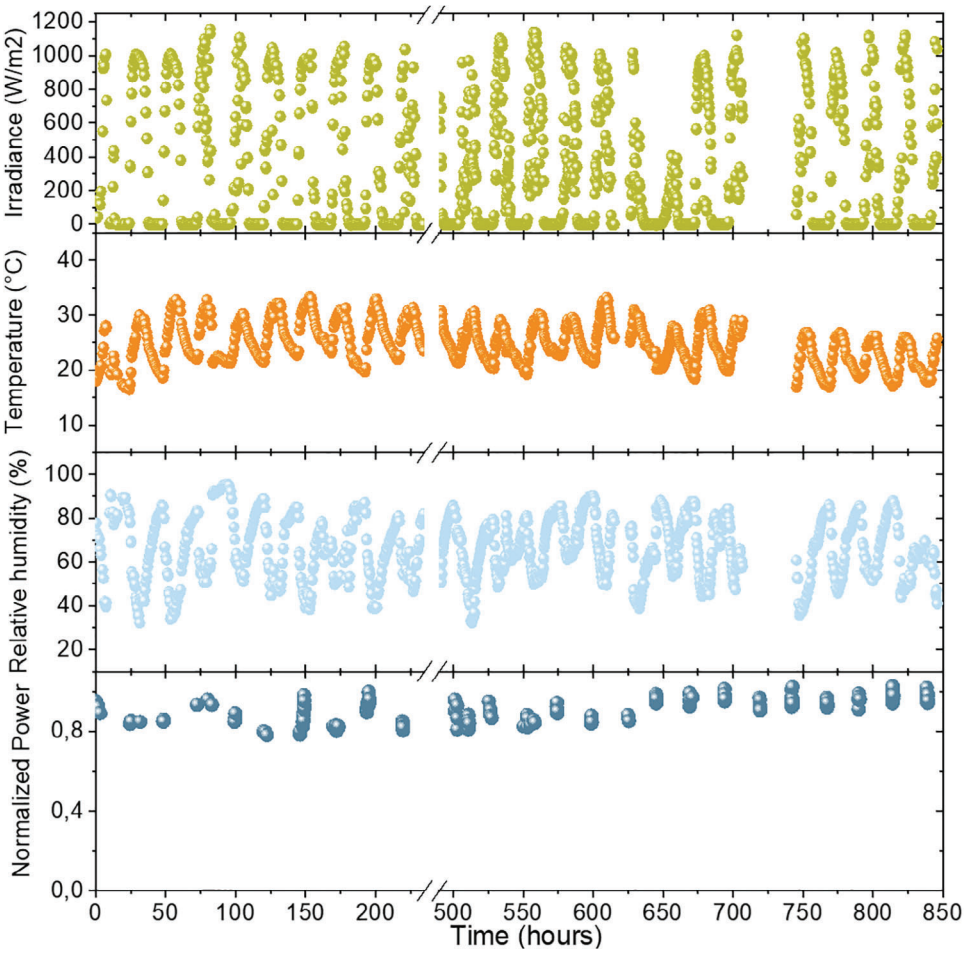

Figure 4. Outdoor stability measurement was carried out with the passivated device following the ISOS-O-1 protocol. Obtained outdoor MPP values of the encapsulated devices (ISOS-O-1 at Barcelona, 41.5021°N, 2.1039°E, Spain) for 850 h. See methods for full details of the MPP tracking protocol, the starting efficiency of the device measured with the solar simulator is 23.49%. Full data is shown in Figure S15 (Supporting Information).

bromide 2D, which is ≈410 nm.[23] To further confirm this assignment, we have prepared a 2D thin film of $MPEA_2PbI_2Br_2$ and compared it with the one obtained by passivation (shown in Figure S13, Supporting Information). The resulting PL shows more than one peak in a given spatial region between 410–520 nm depending on the Br/I ratio.[24]

Overall, the PL and GIWAXS data confirmed that a mixed halide phase is formed from the perovskite surface to the bulk. We suggest that this is related to the fact that the MPEABr salt reacts with the excess of lead iodide present in the precursor solution and, due to thermodynamically favored miscibility between Br and I, Br can enter in the structure creating such a mixed halide phase. To understand the effect of the penetration of the $MPEA_2PbBr_4$ rich-phase in the perovskite bulk, we measure the PL lifetime (Figure 3c) and PLQY (Figure 3d). Figure 3c displays the PL decay after pulsed photoexcitation (at 470 nm wavelength)[25] of both reference and 4-MPEABr-based film. From the passivated films, the charge carrier lifetime elongates from 17.3 ns to 74.2 ns (see Table in Figure S14, Supporting Information). This indicates that the $MPEA_2PbBr_4$ rich-phase also affects the bulk improving the overall quality of the perovskite film.[26,27] In agreement, Figure 3d shows a 3 × increase in the PLQY, confirming, along with the device results, a beneficial effect of the Br-based 2D passivation.

Finally, to test the stability of our cells, we performed outdoor stability analysis according to the ISOS-O-1 protocol.[28] The samples were analyzed after careful encapsulation and the stability test was carried out at Barcelona, Spain, 41.5021°N, 2.1039°E. Notably, these are the optimal conditions for an accelerated test, mimicking real solar cell operation. **Figure 4** shows a minimal loss in stability of the devices. Indeed, during the outdoor Maximum Power Point (MPP) tracking, devices showed stable performance after 850 h in summertime conditions, which entail ambient temperatures ranging from 15–35 °C and relative humidity (RH) between 40–90%. The high stability of the MPEABr devices was strictly related to its minimal hysteresis and passivated defects, as confirmed by PLQY analysis, which are key aspects to consider in order to improve the long-term stability of perovskite solar cells.

3. Conclusion

In conclusion, we demonstrated an innovative method of 2D/3D passivation leading to the formation of a compositionally graded

© 2024 The Author(s). Advanced Energy Materials published by Wiley-VCH GmbH

interface, which had a double beneficial role on the device performances. Using a Br- based salt precursor we induced the formation of the $PEA_2Pb(I_xBr_{1-x})_4$ 2D phase where Br substituted I in the inorganic structure. Such 2D structure formed a non-homogeneous layer on the top surface, responsible for the enhancement in the device V_{OC} and FF. The bulk passivation effect of the halide perovskite with the 2D phase it was responsible for the observed increase in the device J_{SC}. Such double passivation allowed us to obtain remarkably highly efficient solar cells with more than 24% efficiency and excellent outdoor stability. Importantly, we demonstrated stability over 1 month preserving the state of the solar cells, enabling them to perform well even under challenging conditions such as hot and rainy days. This is crucial to assess the validity of perovskite technology for the near future realization of a marketable technology.

4. Experimental Section

All solvents and chemicals were used as purchased without further purification. Acetone (extra pure, 99+%), isopropanol (IPA, 99.5 + %), and chlorobenzene (CB, extra dry, 99.8%) were purchased from Acros Organics. Tin (IV) oxide (SnO_2 15% in H_2O) and N,N-dimethylformamide (DMF, anhydrous, 99.8%) were purchased from Alfa Aesar. Dimethyl sulfoxide (DMSO, anhydrous, ≥99.9%), methylammonium chloride MACl, N2,N2,N2′,N2′,N7,N7,N7′,N7′-octakis(4-methoxyphenyl)-9,9′-spirobi[9H-fluorene]-2,2′,7,7′-tetramine (Spiro-OMeTAD, 99%, HPLC), Bis(trifluoromethane)sulfonimide lithium salt (Li-salt, 99.95%), acetonitrile (ACN, anhydrous, 99.8%), and 4-tert-butylpyridine (4-tBP,98%) were purchased from Sigma-Aldrich. Lead iodide (PbI_2, >98.0%) was purchased from TCI. Formamidinium iodide (FAI, >99.99%) and 4MPEABr were purchased from GreatCell Solar Materials. For the fabrication of PSCs, indium tin oxide (ITO)-coated glass substrates were consecutively cleaned in acetone and IPA by ultrasonicating for 15 min for each solvent. Substrates were dried with N_2 airflow and treated for 10 min in an oxygen-plasma cleaner (ZEPTO, Diener Electronic). SnO_2 colloidal dispersion was diluted to 10% in water and KI was added with a concentration of 3 mg ml^{-1} and 40 µL were spin-coated onto ITO/glass substrates and annealed at 150 °C for 30 min. SnO_2-coated substrates were subjected to UV-ozone treatment for 30 min.

The perovskite precursor solution (1.2 M) was prepared by dissolving PbI_2 and FAI powders in a DMF/DMSO = 4/1 solution with 5% PbI_2 excess. For bulk treatment, 35 mol% of MACl was added to the solution.[29] 25 µL of the final solution were deposited on the SnO_2-coated substrates and spin-coated with a three-step procedure: in the first step substrates were spinned at 1000 rpm for 12 s, the second step proceeded at 5000 rpm for 27 s, while the last step was a speed reduction of 4 s. 9 s after the beginning of the second step, 150 µL of CB were dropped onto the spinning substrate for an antisolvent procedure. Subsequently, substrates were annealed at 150 °C for 10 min. For the surface passivation of the perovskite, 50 µL of a solution 0.01 M of MePEABr in IPA was dynamically spin-coated onto the perovskite layer at 5000 rpm for 30 s. To fabricate the HTL, Spiro-OMeTAD was dissolved in CB to produce an 80 mg mL^{-1} solution. The solution was doped by adding 17.5 µL of Li-salt dissolved in ACN (520 mg mL^{-1} in ACN) and 28.8 µL of 4-tBP to 1 mL of Spiro-OMeTAD solution in CB. 10 µL of the final solution were spin-coated onto the perovskite layer. Finally, 80 nm of Au was thermally evaporated on the device. The evaporation speed was adjusted to 0.01 nm s^{-1} for the first 5 nm, 0.02 nm s^{-1} from 5 to 15 nm, and 0.08 nm s^{-1} for the rest of the procedure.

Devices were characterized through current density voltage measurements performed in ambient conditions under simulated AM1.5 light with an intensity of 100 mW cm^{-2} (Wavelabs-Sinus 70). The intensity was calibrated using a Si reference cell. Cells were scanned using a Keithley 2450 source-meter backward and forward from 1.2 to −0.1 V, with a scanning velocity of 100 mV s^{-1}. The pixel area was 3 by 1.5 mm. The stability measurements were performed at the maximum power point under ambient air_2 using a stability box (Litos Lite) from Fluxim, coupled with a Wavelabs solar simulator continuously illuminating the devices. The spectrum used for the stability measurements was the same as the current density voltage measurements. IPCE measurements were performed in ambient air conditions with a Cicci Research Arkeo steady-state tests module. The wavelength scan range was set between 300–900 nm. TPV analyses were performed in ambient air conditions with a Cicci Research Arkeo transient tests module. Measurements were conducted under constant 1 sun illumination and the constant bias was perturbed with short light pulses of 200 µs width. MPP tracking measurements were operated in an inert atmosphere (0% relative humidity, 0% H_2O, 0% O_2) with Fluxim- Lithos Lite, employing a scan rate of 10.0 mV s^{-1} over a range of −0.1—1.2 V. During measurements, a shadow mask of 1.25 mm^2 area was used to cover the devices. PL emission maps were acquired using a wide-field, hyperspectral imaging microscope (Photon, etc. IMA VIS). The maps were detected with a front-illuminated, low-noise charged-coupled device camera that was thermoelectrically cooled down to 0 °C. A power-tunable 405 nm laser with an intensity of 100 mW cm^{-2} (spot size diameter is ≈150 µm) was used as the excitation source for PL. To block the 405 nm laser reflection, a 420 nm long-pass filter was placed in the detection pathway. XPS and UPS were conducted by employing SPECS Phoibos 150 hemispherical energy analyzer with X-ray beam of Al Kα with a beam width of 100 µm equipped with auto-neutralization and total energy resolution of 2.9 meV. The spectra were calibrated regarding the atomic orbital of C 1s 284.8 eV. GIWAXS data was collected at the I07 Surface and Interface Diffraction beamline at the Diamond Light Source (Didcot, UK). The beam energy was 10 keV (1.239841 Å). The scattered beam was collected by a Pilatus 2 M large area detector at a sample-detector distance of 404 mm and calibrated with a lanthanum hexaboride (LaB6) sample. The incidence angles were scanned from 0.004° to 0.6° with a 0.02° step and frame exposure of 1 s to gather diffraction patterns from both surface and bulk areas of the films. The sample chamber was continuously purged with a 2 l min^{-1} He flow. Data was processed with the DAWN software package. To determine the X-ray penetration depth was first calculated the density of a general cubic $FAPbI_3$ from the lattice parameter 6.36 Å[30] and the atomic masses, which is ≈ 4 gm × cm^{-3}, and then use the database from the Center for X-ray Optics of the Lawrence Berkeley National Laboratory to obtain a match between grazing incidence angle and attenuation length. The devices used for the stability measurement had an active area of 21 cm^2 and were encapsulated with UV epoxy glue. First metal frameworks were connected to the contacts of the devices, then the active area was covered with a UV-curing epoxy and then the top glass was placed and exposed to a UV light source for 10 min. For the study, ISOS-O protocol was used. The missing data are due to maintenance-related power shutdowns on site and after "*" in Figure 4 the device had a lower power respect with the beginning also due to the power shutdown, but no drop in performance due to degradation is visible on the device.

Supporting Information

Supporting Information is available from the Wiley Online Library or from the author.

Acknowledgements

M.D. and R.P. contributed equally to this work. Authors acknowledge the European Research Council (ERC) Starting Grant 2018 under the European Union's Horizon 2020 research and innovation program (Grant Agreement No. 802862) that founded the "HY-NANO". The authors are grateful to the project for infrastructures funded by Regione Lombardia RL3776. The authors are also thankful to The Ministero dell'Università e della Ricerca (MUR), University of Pavia through the program "Dipartimenti di Eccellenza 2023–2027" for funding and FARE (Framework per

© 2024 The Author(s). Advanced Energy Materials published by Wiley-VCH GmbH

l'Attrazione e Il Rafforzamento delle Eccellenze per la Ricerca in Italia) Project EXPRESS (Exploring photo ferroelectricity in halide perovskites for optoelectronics) "Development and characterization of halide perovskites for photo ferroelectrics applications". G.G. and M.D. acknowledges the GOPV project (CSEAA_00011), which received funds from Bando Ricerca di Sistema—CSEA—TIPO A Piano Triennale 2019–2021 Decreto direttoriale 27 Ottobre 2021 del Ministero della Transizione Ecologica; MASE-(ex MITE); The authors acknowledge the European Research Council (ERC) under the European Union's Horizon 2020 research and innovation program (HYPERION, grant agreement No. 756962), and the Engineering and Physical Sciences Research Council (EPSRC) (grant agreement No. EP/V027131/1). S.D.S. acknowledges the Royal Society and Tata Group (grant no. UF150033). Authors acknowledge and thank Diamond Light Source for granting beamtime at I07 (proposal number SI32266-1).

Open access publishing facilitated by Universita degli Studi di Pavia, as part of the Wiley - CRUI-CARE agreement.

Conflict of Interest

The authors declare no conflict of interest.

Data Availability Statement

The data that support the findings of this study are available from the corresponding author upon reasonable request.

Keywords

low-dimensional perovskite, mixed-halide composition, perovskite, solar cells

Received: September 27, 2024
Revised: December 12, 2024
Published online:

[1] D. Ramírez, F. Jaramillo, *Revista Facultad de Ingenieria* **2021**, 67.
[2] X. Li, J. M. Hoffman, M. G. Kanatzidis, *Chem. Rev.* **2021**, *121*, 2230.
[3] V. Larini, M. Degani, G. Pica, C. Ding, Z. Andaji-Garmaroudi, F. Faini, S. D. Stranks, C. Q. Ma, G. Grancini, *Sol. RRL* **2022**, 6.
[4] M. Degani, Q. An, M. Albaladejo-Siguan, Y. J. Hofstetter, C. Cho, F. Paulus, G. Grancini, Y. Vaynzof, *Sci. Adv* **2021**, *7*, 7930.
[5] S. Teale, M. Degani, B. Chen, E. H. Sargent, G. Grancini, *Nat. Energy* **2024**, *9*, 779.
[6] D. W. deQuilettes, J. J. Yoo, R. Brenes, F. U. Kosasih, M. Laitz, B. D. Dou, D. J. Graham, K. Ho, Y. Shi, S. S. Shin, C. Ducati, M. G. Bawendi, V. Bulović, *Nat. Energy* **2024**, *9*, 457.
[7] P. Zhu, S. Gu, X. Luo, Y. Gao, S. Li, J. Zhu, H. Tan, *Adv. Energy Mater.* **2020**, *10*, 1903083.
[8] C. Yang, H. Wang, Y. Miao, C. Chen, M. Zhai, Q. Bao, X. Ding, X. Yang, M. Cheng, **2024**, *14*, 0.
[9] T. Ye, A. Bruno, G. Han, T. M. Koh, J. Li, N. F. Jamaludin, C. Soci, S. G. Mhaisalkar, W. L. Leong, *Adv. Funct. Mater.* **2018**, *28*, 1801654.
[10] C. Zhang, S. Wu, L. Tao, G. M. Arumugam, C. Liu, Z. Wang, S. Zhu, Y. Yang, J. Lin, X. Liu, R. E. I. Schropp, Y. Mai, *Adv. Energy Mater.* **2020**, *10*, 2002004.
[11] M. A. Mahmud, H. T. Pham, T. Duong, Y. Yin, J. Peng, Y. Wu, W. Liang, L. Li, A. Kumar, H. Shen, D. Walter, H. T. Nguyen, N. Mozaffari, G. D. Tabi, G. Andersson, K. R. Catchpole, K. J. Weber, T. P. White, *Adv. Funct. Mater.* **2021**, *31*, 2104251.
[12] D. Yu, F. Cao, J. Liao, B. Wang, C. Su, G. Xing, *Nat. Commun.* **2022**, *13*, 6229.
[13] L. Krückemeier, Z. Liu, T. Kirchartz, U. Rau, *Adv. Mater.* **2023**, *35*, 2300872.
[14] R. Hidayat, A. Asma Nurunnizar, A. Fariz, E. Septa Rosa, T. Oizumi, A. Fujii, M. Ozaki, **2020**, *10*, 19179.
[15] M. Liao, B. Bin Yu, Z. Jin, W. Chen, Y. Zhu, X. Zhang, W. Yao, T. Duan, I. Djerdj, Z. He, *ChemSusChem* **2019**, *12*, 5007.
[16] Y. J. Hofstetter, I. García-Benito, F. Paulus, S. Orlandi, G. Grancini, Y. Vaynzof, *Front Chem* **2020**, *8*, 66.
[17] M. Liao, B. Bin Yu, Z. Jin, W. Chen, Y. Zhu, X. Zhang, W. Yao, T. Duan, I. Djerdj, Z. He, *ChemSusChem* **2019**, *12*, 5007.
[18] https://www.nanoge.org/proceedings/IPEROP24/655b372e9f2cc075006d1acf (accessed: January 2024).
[19] https://henke.lbl.gov/optical_constants/atten2.html, (visited on June 2024).
[20] D. W. deQuilettes, J. J. Yoo, R. Brenes, F. U. Kosasih, M. Laitz, B. D. Dou, D. J. Graham, K. Ho, Y. Shi, S. S. Shin, C. Ducati, M. G. Bawendi, V. Bulović, *Nat. Energy* **2024**, *9*, 457.
[21] N. Phung, A. Bracesco, M. Creatore, Y. Zhu, M. Hu, M. Xu, B. Zhang, F. Huang, Y. B. Cheng, J. Lu, *Mater. Futures* **2022**, *1*, 042102.
[22] S. Cacovich, G. Vidon, M. Degani, M. Legrand, L. Gouda, J. B. Puel, Y. Vaynzof, J. F. Guillemoles, D. Ory, G. Grancini, *Nat. Commun.* **2022**, *13*, 2868.
[23] Y. Zhang, Y. Liu, Z. Xu, H. Ye, Q. Li, M. Hu, Z. Yang, S. (Frank) Liu, *J. Mater. Chem. C* **2019**, *7*, 1584.
[24] A. Zanetta, Z. Andaji-Garmaroudi, V. Pirota, G. Pica, F. U. Kosasih, L. Gouda, K. Frohna, C. Ducati, F. Doria, S. D. Stranks, G. Grancini, A. Zanetta, Z. Andaji-Garmaroudi, V. Pirota, G. Pica, L. Gouda, F. Doria, G. Grancini, K. Frohna, S. D. Stranks, F. U. Kosasih, C. Ducati, *Adv. Mater.* **2022**, *34*, 2105942.
[25] G. Pica, D. Bajoni, G. Grancini, *Cite as: Struct. Dyn* **2022**, *9*, 11101.
[26] A. A. B. Baloch, F. H. Alharbi, G. Grancini, M. I. Hossain, M. K. Nazeeruddin, N. Tabet, *J. Phys. Chem. C* **2018**, *122*, 26805.
[27] H. Yu, F. Wang, F. Xie, W. Li, J. Chen, N. Zhao, *Adv. Funct. Mater.* **2014**, *24*, 7102.
[28] M. V. Khenkin, E. A. Katz, A. Abate, G. Bardizza, J. J. Berry, C. Brabec, F. Brunetti, V. Bulović, Q. Burlingame, A. Di Carlo, R. Cheacharoen, Y. B. Cheng, A. Colsmann, S. Cros, K. Domanski, M. Dusza, C. J. Fell, S. R. Forrest, Y. Galagan, D. Di Girolamo, M. Grätzel, A. Hagfeldt, E. Hauff, H. Hoppe, J. Kettle, H. Köbler, M. S. Leite, S. Liu, Y. L. Loo, J. M. Luther, et al., *Nat. Energy* **2020**, *5*, 35.
[29] R. Pallotta, M. Degani, F. Toniolo, S. Cavalli, F. Turci, W. H. Bi, A. Girella, C. Milanese, A. Schüler, A. Magrez, G. Grancini, *Mat. T. Adv.* **2024**, *24*, 100541.
[30] M. T. Weller, O. J. Weber, J. M. Frost, A. Walsh, *J. Phys. Chem. Lett.* **2015**, *6*, 3209.

© 2024 The Author(s). Advanced Energy Materials published by Wiley-VCH GmbH